High-statistics study of neutral-pion pair production in two-photon collisions

S. Uehara,[8] Y. Watanabe,[14] H. Nakazawa,[23] H. Aihara,[40] K. Arinstein,[1,29] V. Aulchenko,[1,29] A. M. Bakich,[36] E. Barberio,[20] K. Belous,[11] V. Bhardwaj,[31] A. Bondar,[1,29] A. Bozek,[26] M. Bračko,[19,13] T. E. Browder,[7] A. Chen,[23] B. G. Cheon,[6] R. Chistov,[12] I.-S. Cho,[44] S.-K. Choi,[5] Y. Choi,[35] M. Dash,[43] S. Eidelman,[1,29] D. Epifanov,[1,29] N. Gabyshev,[1,29] P. Goldenzweig,[2] H. Ha,[15] J. Haba,[8] B.-Y. Han,[15] K. Hayasaka,[21] H. Hayashii,[22] M. Hazumi,[8] Y. Hoshi,[39] W.-S. Hou,[25] H. J. Hyun,[16] K. Inami,[21] A. Ishikawa,[32] Y. Iwasaki,[8] N. J. Joshi,[37] D. H. Kah,[16] N. Katayama,[8] T. Kawasaki,[28] H. Kichimi,[8] H. O. Kim,[16] Y. I. Kim,[16] Y. J. Kim,[4] S. Korpar,[19,13] P. Križan,[18,13] P. Krokovny,[8] A. Kuzmin,[1,29] Y.-J. Kwon,[44] M. J. Lee,[34] T. Lesiak,[26,3] Y. Liu,[21] D. Liventsev,[12] R. Louvot,[17] S. McOnie,[36] H. Miyata,[28] R. Mizuk,[12] Y. Nagasaka,[9] M. Nakao,[8] S. Nishida,[8] K. Nishimura,[7] O. Nitoh,[42] S. Ogawa,[38] T. Ohshima,[21] S. Okuno,[14] P. Pakhlov,[12] G. Pakhlova,[12] C. W. Park,[35] H. Park,[16] H. K. Park,[16] R. Pestotnik,[13] L. E. Piilonen,[43] A. Poluektov,[1,29] H. Sahoo,[7] Y. Sakai,[8] O. Schneider,[17] K. Senyo,[21] M. Shapkin,[11] J.-G. Shiu,[25] B. Shwartz,[1,29] M. Starič,[13] T. Sumiyoshi,[41] M. Tanaka,[8] Y. Teramoto,[30] I. Tikhomirov,[12] T. Uglov,[12] Y. Unno,[6] S. Uno,[8] Y. Usov,[1,29] G. Varner,[7] K. Vervink,[17] A. Vinokurova,[1,29] C. H. Wang,[24] P. Wang,[10] B. D. Yabsley,[36] Y. Yamashita,[27] C. C. Zhang,[10] Z. P. Zhang,[33] V. Zhilich,[1,29] V. Zhulanov,[1,29] T. Zivko,[13] A. Zupanc,[13] and O. Zyukova[1,29]

(Belle Collaboration)

[1]*Budker Institute of Nuclear Physics, Novosibirsk*
[2]*University of Cincinnati, Cincinnati, Ohio 45221*
[3]*T. Kościuszko Cracow University of Technology, Krakow*
[4]*The Graduate University for Advanced Studies, Hayama*
[5]*Gyeongsang National University, Chinju*
[6]*Hanyang University, Seoul*
[7]*University of Hawaii, Honolulu, Hawaii 96822*
[8]*High Energy Accelerator Research Organization (KEK), Tsukuba*
[9]*Hiroshima Institute of Technology, Hiroshima*
[10]*Institute of High Energy Physics, Chinese Academy of Sciences, Beijing*
[11]*Institute of High Energy Physics, Protvino*
[12]*Institute for Theoretical and Experimental Physics, Moscow*
[13]*J. Stefan Institute, Ljubljana*
[14]*Kanagawa University, Yokohama*
[15]*Korea University, Seoul*
[16]*Kyungpook National University, Taegu*
[17]*École Polytechnique Fédérale de Lausanne (EPFL), Lausanne*
[18]*Faculty of Mathematics and Physics, University of Ljubljana, Ljubljana*
[19]*University of Maribor, Maribor*
[20]*University of Melbourne, School of Physics, Victoria 3010*
[21]*Nagoya University, Nagoya*
[22]*Nara Women's University, Nara*
[23]*National Central University, Chung-li*
[24]*National United University, Miao Li*
[25]*Department of Physics, National Taiwan University, Taipei*
[26]*H. Niewodniczanski Institute of Nuclear Physics, Krakow*
[27]*Nippon Dental University, Niigata*
[28]*Niigata University, Niigata*
[29]*Novosibirsk State University, Novosibirsk*
[30]*Osaka City University, Osaka*
[31]*Panjab University, Chandigarh*
[32]*Saga University, Saga*
[33]*University of Science and Technology of China, Hefei*
[34]*Seoul National University, Seoul*
[35]*Sungkyunkwan University, Suwon*
[36]*University of Sydney, Sydney, New South Wales*
[37]*Tata Institute of Fundamental Research, Mumbai*
[38]*Toho University, Funabashi*
[39]*Tohoku Gakuin University, Tagajo*

[40]*Department of Physics, University of Tokyo, Tokyo*
[41]*Tokyo Metropolitan University, Tokyo*
[42]*Tokyo University of Agriculture and Technology, Tokyo*
[43]*IPNAS, Virginia Polytechnic Institute and State University, Blacksburg, Virginia 24061*
[44]*Yonsei University, Seoul*

(Received 22 January 2009; published 25 March 2009)

The differential cross sections for the process $\gamma\gamma \to \pi^0\pi^0$ have been measured in the kinematic range 0.6 GeV $< W <$ 4.1 GeV, $|\cos\theta^*| < 0.8$ in energy and pion scattering angle, respectively, in the $\gamma\gamma$ center-of-mass system. The results are based on a 223 fb^{-1} data sample collected with the Belle detector at the KEKB e^+e^- collider. The differential cross sections are fitted in the energy region 1.7 GeV $< W <$ 2.5 GeV to confirm the two-photon production of two pions in the G wave. In the higher-energy region, we observe production of the χ_{c0} charmonium state and obtain the product of its two-photon decay width and branching fraction to $\pi^0\pi^0$. We also compare the observed angular dependence and ratios of cross sections for neutral-pion and charged-pion pair production to QCD models. The energy and angular dependence above 3.1 GeV are compatible with those measured in the $\pi^+\pi^-$ channel, and in addition we find that the cross section ratio, $\sigma(\pi^0\pi^0)/\sigma(\pi^+\pi^-)$, is $0.32 \pm 0.03 \pm 0.05$ on average in the 3.1–4.1 GeV region.

DOI: 10.1103/PhysRevD.79.052009 PACS numbers: 13.20.Gd, 13.60.Le, 13.66.Bc, 14.40.Cs

I. INTRODUCTION

Measurements of exclusive hadronic final states in two-photon collisions provide valuable information concerning the physics of light and heavy-quark resonances, perturbative and nonperturbative QCD, and hadron-production mechanisms. So far, we have measured the production cross sections for charged-pion pairs [1,2], charged- and neutral-kaon pairs [2–4], and proton-antiproton pairs [5]. We have also analyzed D-meson-pair production and observe a new charmonium state [6]. Recently, we have presented a measurement of neutral-pion pair production based on a data sample corresponding to an integrated luminosity of 95 fb^{-1} [7]. We have carried out an analysis in the energy range $W < 1.6$ GeV to extract information on light quark resonances from the energy and angular dependence of the differential cross sections, by fitting to the resonance parameters of the $f_0(980)$, $f_2(1270)$, and additional hypothetical resonances. The statistics of these measurements is 2 to 3 orders of magnitude higher than in the pre-B-factory measurements [8], opening a new era in studies of two-photon physics.

Here we present measurements of the differential cross sections, $d\sigma/d|\cos\theta^*|$, for the process $\gamma\gamma \to \pi^0\pi^0$ in a wide two-photon center-of-mass (c.m.) energy (W) range from 0.6 to 4.1 GeV, and in the c.m. angular range, $|\cos\theta^*| < 0.8$. We use a 223 fb^{-1} data sample, which is more than twice as large as that in our previous analysis [7]. We focus on the range $W > 1.4$ GeV, where the previous data were statistically limited.

In the intermediate energy range (1.0 GeV $< W <$ 2.4 GeV), production of two pions is dominated by intermediate resonances. For ordinary $q\bar{q}$ mesons in isospin conserving decays to $\pi\pi$, the only allowed I^GJ^{PC} states produced by two photons are $0^+(\text{even})^{++}$, that is, $f_{J=\text{even}}$ mesons. Several mesons with these quantum numbers are suggested by results of hadron-beam or charmonium decay experiments in the 1.5–2.2 GeV region. However, none of them have been firmly established in two-photon processes, which are sensitive to the internal quark structure of the meson. In addition, the $\pi^0\pi^0$ channel has two advantages in the study of resonances: a smaller contribution from the continuum is expected in it than in the $\pi^+\pi^-$ channel; and the angular coverage is larger ($|\cos\theta^*| < 0.8$ instead of 0.6).

At higher energies ($W > 2.4$ GeV), we can invoke a quark model. In leading-order calculations [9–11], which take into account the spin correlation between quarks, the $\pi^0\pi^0$ cross section is predicted to be much smaller than that of $\pi^+\pi^-$, suggesting a ratio of $\pi^0\pi^0$ to $\pi^+\pi^-$ cross sections around 0.04–0.07. However, higher-order or nonperturbative QCD effects can modify this prediction. For example, the handbag model, which considers soft hadron exchange, predicts the same amplitude for the two processes, and thus the expected ratio is 0.5 [12]. Analyses of energy and angular distributions of the cross sections are essential for determining the properties of the observed resonances and for testing the validity of QCD models.

The organization of this article is as follows. In Sec. II, a brief description of the Belle detector is given. Section III explains the procedure used to obtain differential cross sections. Section IV is devoted to results on the two-photon production of two pions in the G wave obtained by fitting differential cross sections in the range 1.7 GeV $< W <$ 2.5 GeV. Section V describes analyses at higher energy. The topics included there are the angular dependence as a function of W, the observation of the χ_{c0} and χ_{c2} charmonia states and the ratio of cross sections for $\pi^0\pi^0$ to $\pi^+\pi^-$ production. Finally, Sec. VI summarizes the results and presents the conclusion of this paper.

TABLE I. Data sample: luminosities and energies.

e^+e^- c.m. energy (GeV)	Luminosity (fb^{-1})	Comment
10.58	179.0	$\Upsilon(4S)$ runs
10.52	19.0	Continuum runs
10.36	2.9	$\Upsilon(3S)$ runs
10.30	0.3	Continuum runs
10.86	21.7	$\Upsilon(5S)$ runs
Total	223.0	

II. EXPERIMENTAL APPARATUS

We use a 223 fb^{-1} data sample from the Belle experiment [13] at the KEKB asymmetric-energy e^+e^- collider [14]. The data were recorded at several e^+e^- c.m. energies summarized in Table I. The difference of the luminosity functions (two-photon flux per e^+e^--beam luminosity) in the measured W regions due to the difference of the beam energies is small (maximum $\pm 4\%$). We combine the results from the different beam energies. The effect on the cross section is less than 0.5%.

The analysis is carried out in the "zero-tag" mode, where neither the recoil electron nor positron are detected. We restrict the virtuality of the incident photons to be small by imposing strict transverse-momentum balance with respect to the beam axis for the final-state hadronic system.

A comprehensive description of the Belle detector is given elsewhere [13]. We mention here only those detector components that are essential for the present measurement. Charged tracks are reconstructed from hit information in the silicon vertex detector and the central drift chamber located in a uniform 1.5 T solenoidal magnetic field. The detector solenoid is oriented along the z axis, which points in the direction opposite to that of the positron beam. Photon detection and energy measurements are performed with a CsI(Tl) electromagnetic calorimeter (ECL).

For this all-neutral final state, we require that there be no reconstructed tracks coming from the vicinity of the nominal collision point. Therefore, the central drift chamber is used for vetoing events with charged track(s). The photons from decays of two neutral pions are detected and their momentum vectors are measured by the ECL. The ECL is also used to trigger signal events.

III. DERIVING DIFFERENTIAL CROSS SECTIONS

The event triggers, data processing, and event selection are the same as those described in Ref. [7]. We derive the c.m. energy W of the two-photon collision from the invariant mass of the two-neutral-pion system. We calculate the cosine $|\cos\theta^*|$ of the π^0 scattering angle in the $\gamma\gamma$ c.m. frame for each event, using the e^+e^- collision axis in the e^+e^- c.m. frame as the reference axis for the polar angle. The possible bias due to the unknown $\gamma\gamma$ collision axis is negligible.

A. Data reduction

We find that the signal candidates in the low energy region ($W < 1.2$ GeV) are considerably contaminated by background. In order to separate the signal and background components, we study the p_t-balance distribution, i.e., the event distribution in $|\sum \boldsymbol{p}_t^*|$. We estimate the p_t-unbalanced background component for $W < 1.2$ GeV in the same manner as in the previous analysis [7] and subtract the yield in the signal region. However, above 1.2 GeV, we cannot quantitatively determine the background contamination because of the small background rate and low statistics of the sample, as well as the uncertainty in the functional form for the signal shape.

Using the ratio of yields between the p_t-balanced and unbalanced regions, we can estimate the backgrounds. In Fig. 1, we plot the W dependence of R defined as

$$R = \frac{Y(0.15\ \mathrm{GeV}/c < |\sum \boldsymbol{p}_t^*| < 0.20\ \mathrm{GeV}/c)}{Y(|\sum \boldsymbol{p}_t^*| < 0.05\ \mathrm{GeV}/c)}, \quad (1)$$

where Y is the yield in the indicated $|\sum \boldsymbol{p}_t^*|$ region. We integrate over all angles in this figure. The main part of the W dependence of R comes from the energy dependence of the momentum resolution. The expected ratio from the pure signal component is shown by the solid line. The signal events for $e^+e^- \to e^+e^-\pi^0\pi^0$ are generated using the TREPS code [15]. All Monte Carlo (MC) events are put through the trigger and detector simulators and the event selection program. The MC events are corrected for MC/data difference in the p_t resolution discussed in the next section. The excess of R over the line (ΔR) is expected to correspond to the contribution from the p_t-unbalanced background. The excess is relatively small above 1.0 GeV, although some fine structure is visible there. In

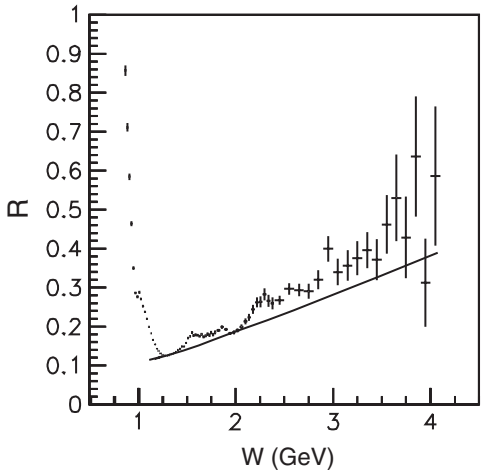

FIG. 1. The yield ratio R in the p_t-unbalanced bin to the p_t-balanced (signal) bin (see text for the exact definition) for the experimental data. The solid line shows the signal component obtained from the signal MC and corrected taking into account the poorer momentum resolution in experimental data.

the range 1.2–3.3 GeV, ΔR ranges between 0.00 and 0.08, and above 3.3 GeV it is in the range from 0.08 to 0.2. From the R values, we estimate that the background contamination in the signal region is $\sim R/4$, which is smaller than 3% for 1.5–3.3 GeV and around 3% for 3.6–4.1 GeV. We subtract 3% for 3.6–4.1 GeV, and assign a 3% systematic error from this source for the full 1.5–4.1 GeV range.

We estimate the invariant-mass resolution from studies of signal-MC and experimental distribution. The true W distribution in the range 0.9 GeV $< W <$ 2.4 GeV is obtained by unfolding the differential cross sections as described in Ref. [7]. For lower energies, $W <$ 0.9 GeV, the effect of the migration is expected to be small because the invariant-mass resolution is much smaller than the bin width. For higher energies, $W >$ 2.4 GeV, where the statistics is relatively low and unfolding would enlarge the errors, we adopt a rather wide bin width (100 MeV) without unfolding. A total of 2.90×10^6 events are selected in the region of 0.6 GeV $< W <$ 4.1 GeV and $|\cos\theta^*| < 0.8$.

B. Calculation of differential cross sections

We determine the efficiency for the signal using a full MC simulation. The MC signal events generated using the TREPS code [15] are isotropically distributed in $|\cos\theta^*|$ at 58 fixed W points between 0.5 and 4.5 GeV. The angular distribution at the generator level does not play a role in the efficiency determination, because we calculate the efficiencies separately in each $|\cos\theta^*|$ bin with a 0.05 width. Samples of 4×10^5 events are generated at each W point. Two sets of different background conditions, which were extracted from the beam collision data, are embedded in the signal-MC data in the detector simulation. To minimize statistical fluctuations in the MC calculation, we fit the numerical results of the trigger efficiency to a two-dimensional empirical function in $(W, |\cos\theta^*|)$.

The efficiency calculated from the signal-MC events is corrected for a systematic difference of the peak widths in the p_t-balance distributions found between the experimental data and the MC events, which is attributed to a difference in the momentum resolution for π^0's. The correction factor is typically 0.95.

The differential cross section for each $(W, |\cos\theta^*|)$ point is given by

$$\frac{d\sigma}{d|\cos\theta^*|} = \frac{\Delta Y - \Delta B}{\Delta W \Delta|\cos\theta^*| \int \mathcal{L} dt L_{\gamma\gamma}(W) \eta}, \qquad (2)$$

where ΔY and ΔB are the signal yield and the estimated p_t-unbalanced background in the bin, ΔW and $\Delta|\cos\theta^*|$ are the bin widths, $\int \mathcal{L} dt$ and $L_{\gamma\gamma}(W)$ are the integrated luminosity and two-photon luminosity function calculated by TREPS [15], respectively, and η is the efficiency including the correction described above. The bin sizes for W and $\Delta|\cos\theta^*|$ are summarized in Table II.

TABLE II. Bin sizes.

W range (GeV)	ΔW (GeV)	$\Delta\|\cos\theta^*\|$
0.6–1.8	0.02	0.05
1.8–2.4	0.04	0.05
2.4–4.1	0.10	0.05

Figure 2 shows the W dependence of the cross section integrated over $|\cos\theta^*| < 0.8$. We have removed the bins in the range 3.3 GeV $< W <$ 3.6 GeV, because we cannot separate the χ_{c0} and χ_{c2} components and the continuum in a model-independent way due to the finite mass resolution and insufficient statistics of the measurement. The cross section in this region is discussed in detail in Sec. V.

We show the angular dependence of the differential cross sections at several W points in Fig. 3. Note that the cross sections in neighboring bins after the unfolding are no longer independent of each other in either central values or size of errors.

The systematic uncertainties for the cross sections arise from various sources; they are listed in Table III together with the estimated values. Uncertainties from the unfolding procedure, using the single value decomposition approach in Ref. [16], are estimated by varying the effective-rank parameter of the decomposition within reasonable bounds.

The total systematic error is obtained by adding the uncertainties in quadrature and is about 10% in the intermediate W region (1.04 GeV $< W <$ 3.0 GeV). It becomes much larger at lower W. At higher W, the systematic error is rather stable, typically about 11%.

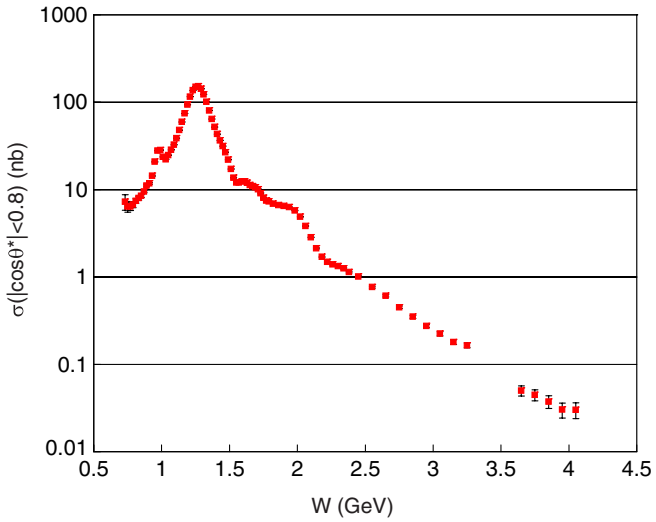

FIG. 2 (color online). The integrated cross section in the angular regions $|\cos\theta^*| < 0.8$. Data points in bins near 3.5 GeV are not shown because of uncertainty from the χ_{cJ} subtraction.

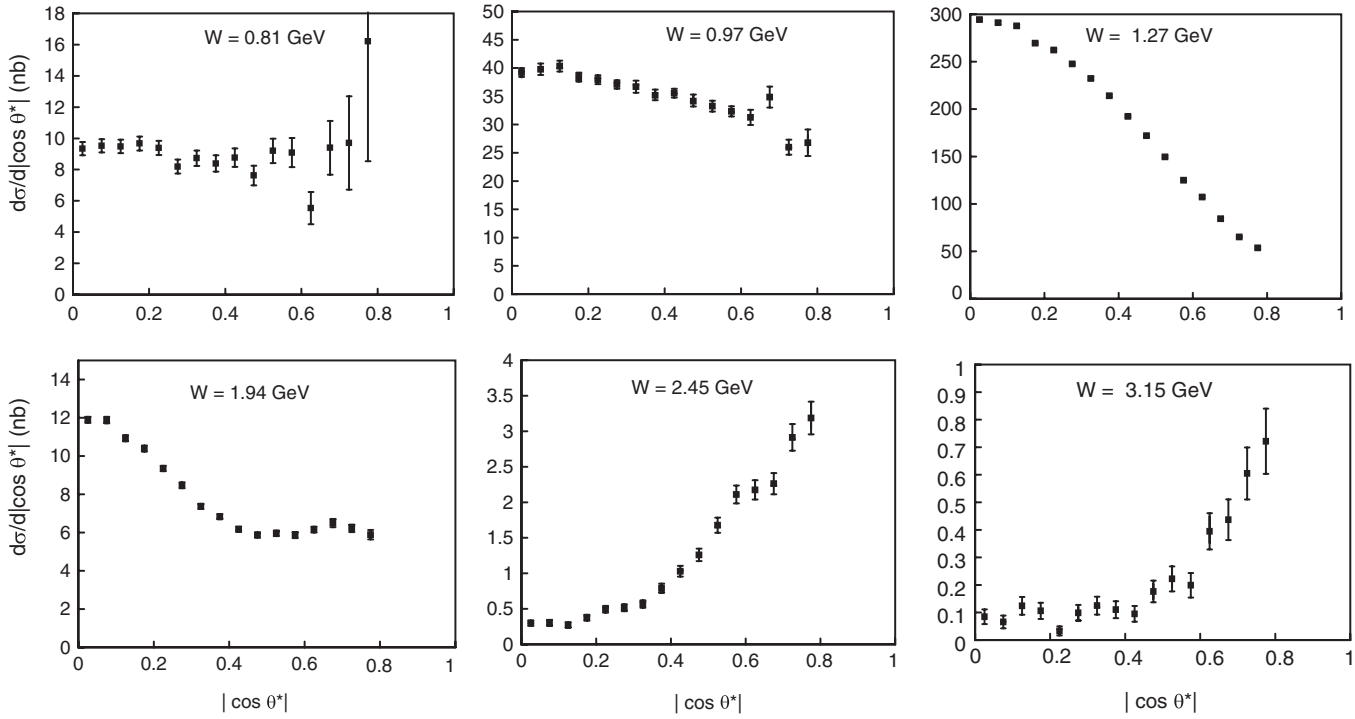

FIG. 3. The differential cross sections for W points indicated. The bin sizes are summarized in Table II.

TABLE III. Systematic errors for the differential cross sections. Ranges of errors are shown when they depend on W.

Source	Error (%)
Trigger efficiency	4–30
π^0 reconstruction efficiency	6
p_t-balance cut	1.5–5
Background subtraction	0–40
Luminosity function	4–5
Overlapping hits from beam background	2–4
Other efficiency errors	4
Unfolding procedure	0–4
Overall	Typically 10–11

IV. STUDY OF G-WAVE ACTIVITY

Previously, we obtained a reasonable fit to a simple model of resonances and smooth backgrounds in the energy region 0.8 GeV $< W <$ 1.6 GeV from the differential cross sections of $\gamma\gamma \to \pi^0\pi^0$ with a 95 fb^{-1} data sample [7]. The clear $f_0(980)$ peak and the large contribution from the $f_2(1270)$ can be fitted with parameters determined from $\pi^+\pi^-$ data [1].

In this section, we concentrate on the G wave, in particular, the $f_4(2050)$ resonance, whose existence is well established, but whose production in two-photon collisions has never been positively identified. We fit the energy region 1.7 GeV $< W <$ 2.5 GeV using a high-statistics sample of 223 fb^{-1} that contains 2.3 times more events than in the previous experiment [7]; the number of events in this region is 155 k.

A. Parametrization of partial wave amplitudes

In the energy region $W \leq 3$ GeV, $J > 4$ partial waves (the next is $J = 6$) may be neglected so that only S, D, and G waves are to be considered. The differential cross section can be expressed as

$$\frac{d\sigma}{d\Omega}(\gamma\gamma \to \pi^0\pi^0) = |SY_0^0 + D_0Y_2^0 + G_0Y_4^0|^2 + |D_2Y_2^2 + G_2Y_4^2|^2, \quad (3)$$

where D_0 and G_0 (D_2 and G_2) denote the helicity 0 (2) components of the D and G waves, respectively, and Y_J^m are the spherical harmonics. Since the $|Y_J^m|$'s are not independent, partial waves cannot be separated using measurements of differential cross sections alone. To overcome this problem, we write Eq. (3) as

$$\frac{d\sigma}{4\pi d|\cos\theta^*|}(\gamma\gamma \to \pi^0\pi^0) = \hat{S}^2|Y_0^0|^2 + \hat{D}_0^2|Y_2^0|^2 + \hat{D}_2^2|Y_2^2|^2 + \hat{G}_0^2|Y_4^0|^2 + \hat{G}_2^2|Y_4^2|^2. \quad (4)$$

The amplitudes $\hat{S}^2$, etc., correspond to the cases where interference terms are neglected; they can be expressed in terms of S, D_0, D_2, G_0, and G_2 [7]. Since squares of spherical harmonics are independent of one another, we can fit differential cross sections at each W to obtain $\hat{S}^2$, $\hat{D}_0^2$, $\hat{D}_2^2$, $\hat{G}_0^2$, and $\hat{G}_2^2$. For $|\cos\theta^*| < 0.7$, the $|Y_4^0|^2$ and $|Y_4^2|^2$ terms are nearly equal, so we fit $\hat{G}_0^2+\hat{G}_2^2$ and $\hat{G}_0^2 - \hat{G}_2^2$ instead. The resulting spectra are shown in Figs. 4 and 5.

We parametrize the partial wave amplitudes in terms of resonances and smooth "backgrounds." Once the functional forms of the amplitudes are fixed, we can use Eq. (3)

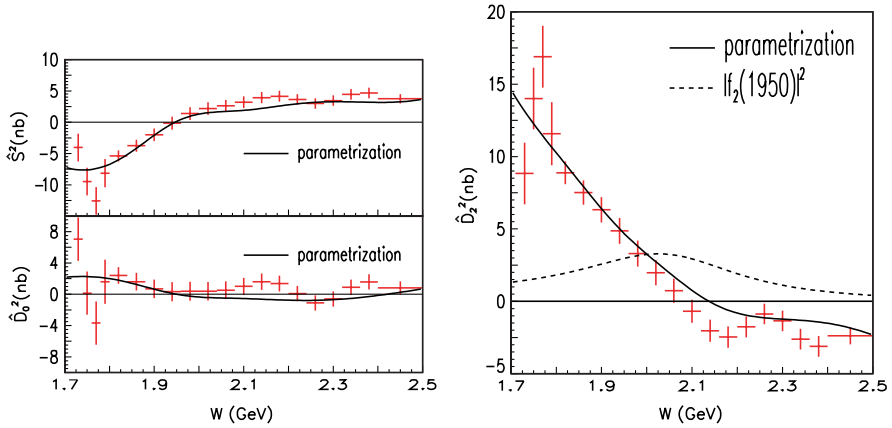

FIG. 4 (color online). Spectrum of $\hat{S}^2$ (top section of left-hand panel), $\hat{D}_0^2$ (bottom section of left-hand panel) and $\hat{D}_2^2$ (right panel) for 1.7 GeV $< W <$ 2.5 GeV and results of parametrization (see text). The error bars shown are diagonal statistical errors.

to fit the differential cross sections. From Fig. 5, it appears that the G wave contributions are nonzero for $W \gtrsim 1.8$ GeV and are dominated by the G_2 wave. Here we assume (and check the necessity of) including the $f_4(2050)$ in the G_2 wave. Since the G_2 wave interferes with the D_2 wave, we include the resonance $f_2(1950)$, which is known to couple to two photons [3,17]. There are several other resonances that might couple to $\gamma\gamma$ and $\pi\pi$ in this mass region, which are listed in Ref. [17]. Here we assume that the $f_2(1950)$ is just an empirical parametrization representing these other resonances; we denote it here as the "$f_2(1950)$."

We parametrize the partial waves as follows:

$$S = B_S, \qquad D_0 = B_{D0}, \qquad D_2 = A_{\text{“}f_2(1950)\text{”}} e^{i\phi_2} + B_{D2},$$
$$G_0 = 0, \qquad G_2 = A_{f_4(2050)} e^{i\phi_4} + B_{G2}, \tag{5}$$

where $A_{\text{“}f_2(1950)\text{”}}$ and $A_{f_4(2050)}$ are the amplitudes of the corresponding resonances; B_S, B_{D0}, B_{D2}, and B_{G2} are nonresonant (background) amplitudes for S, D_0, D_2, and G_2 waves; and ϕ_2 and ϕ_4 are the phases of resonances relative to background amplitudes. We assume that $G_0 = 0$ and

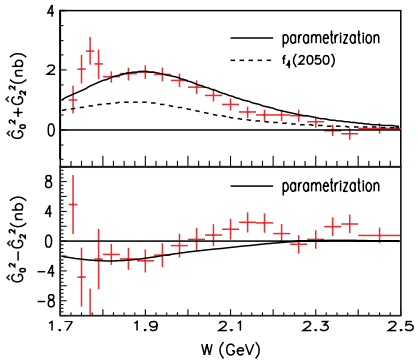

FIG. 5 (color online). Spectrum of $\hat{G}_0^2 + \hat{G}_2^2$ (top section) and $\hat{G}_0^2 - \hat{G}_2^2$ (bottom section) for 1.7 GeV $< W <$ 2.5 GeV and fitted curves (see text). The error bars shown are diagonal statistical errors.

that G_2 consists only of the $f_4(2050)$ and a smooth background.

The relativistic Breit-Wigner resonance amplitude $A_R(W)$ for a spin-J resonance R of mass m_R is given by

$$A_R^J(W) = \sqrt{\frac{8\pi(2J+1)m_R}{W}} \frac{\sqrt{\Gamma_{\text{tot}}\Gamma_{\gamma\gamma}\mathcal{B}(\pi^0\pi^0)}}{m_R^2 - W^2 - im_R\Gamma_{\text{tot}}}. \tag{6}$$

The resonance parameters given in Ref. [17] for the $f_2(1950)$ and $f_4(2050)$ are summarized in Table IV. We assume an energy-independent width for the "$f_2(1950)$" and $f_4(2050)$ because most of their individual decay fractions are unknown.

The background amplitudes are parametrized as follows:

$$\begin{aligned} B_S &= a_{sr}(W - W_0)^2 + b_{sr}(W - W_0) + c_{sr} \\ &\quad + i(a_{si}(W - W_0)^2 + b_{si}(W - W_0) + c_{si}), \\ B_{D0} &= a_0(W - W_0)^2 + b_0(W - W_0) + c_0, \\ B_{D2} &= a_{2r}(W - W_0)^2 + b_{2r}(W - W_0) + c_{2r} \\ &\quad + i(a_{2i}(W - W_0)^2 + b_{2i}(W - W_0) + c_{2i}), \\ B_{G2} &= a_g(W - W_0)^2 + b_g(W - W_0) + c_g \end{aligned} \tag{7}$$

where $W_0 = 1.7$ GeV. The background amplitudes D_0 and G_2 are taken to be real by definition. The other background amplitudes are assumed to be quadratic in W for both their real and imaginary parts. We fix $B_{G2} = 0$ at $W = 1.7$ GeV

TABLE IV. Parameters of the $f_2(1950)$ and $f_4(2050)$ [17].

Parameter	$f_2(1950)$	$f_4(2050)$	Unit
Mass	1944 ± 12	2018 ± 11	MeV/c^2
Width	472 ± 18	237 ± 18	MeV
$\mathcal{B}(\pi\pi)$	Seen	17.0 ± 1.5	%
$\mathcal{B}(K\bar{K})$	Seen	$0.68^{+0.34}_{-0.18}$	%
$\mathcal{B}(\eta\eta)$	Seen	0.21 ± 0.08	%
$\mathcal{B}(\gamma\gamma)$	Seen	Unknown	

TABLE V. Fitted parameters.

Parameter	Nominal	Fixed $f_4(2050)$	No $f_4(2050)$	No "$f_2(1950)$"	Unit
Mass($f_4(2050)$)	1885^{+14}_{-13}	2025 (fixed)	...	2052 ± 6	MeV/c^2
$\Gamma_{\rm tot}(f_4(2050))$	453 ± 20	225 (fixed)	...	257^{+8}_{-7}	MeV
$\Gamma_{\gamma\gamma}\mathcal{B}(\pi^0\pi^0)$	$7.7^{+1.2}_{-1.1}$	11.8 ± 0.2	0 (fixed)	$14.2^{+0.9}_{-0.8}$	eV
Mass("$f_2(1950)$")	2038^{+13}_{-11}	2026^{+2}_{-1}	2114^{+11}_{-13}	...	MeV/c^2
$\Gamma_{\rm tot}$("$f_2(1950)$")	441^{+27}_{-25}	237 ± 4	587^{+20}_{-1}	...	MeV
$\Gamma_{\gamma\gamma}\mathcal{B}(\pi^0\pi^0)$	54^{+23}_{-14}	76^{+48}_{-46}	334^{+79}_{-77}	0 (fixed)	eV
$\chi^2(ndf)$	323.2 (311)	594.4 (313)	1397.8 (315)	2306.8 (315)	

($c_g = 0$) to reduce the number of parameters; leaving c_g free does not improve the fits.

B. Fit results

We minimize χ^2 defined as

$$\chi^2 = \sum_{i,j}\left(\frac{\frac{d\sigma}{d|\cos\theta^*|}(W_i,|\cos\theta^*|_j)_{\rm data} - \frac{d\sigma}{d|\cos\theta^*|}(W_i,|\cos\theta^*|_j)_{\rm pred}}{\Delta\frac{d\sigma}{d|\cos\theta^*|}(W_i,|\cos\theta^*|_j)_{\rm data}}\right)^2, \tag{8}$$

where the summation is over $(W_i, |\cos\theta^*|_j)$ bins, $d\sigma/d|\cos\theta^*|(W_i, |\cos\theta^*|_j)_{\rm data(pred)}$ is the cross section data [prediction using Eq. (5)] at a bin $(W_i, |\cos\theta^*|_j)$, and the denominator is the estimated statistical error.

When the mass and width of the $f_4(2050)$ are fixed to the values given in the PDG tables [17] as summarized in Table IV, then the fit is very poor yielding $\chi^2(ndf) = 594.4(313)$ (see Table V). This is to be compared with 323.2 (311) obtained when the mass and width are floated. In this paper we quote the results of the fits with the mass and width of the $f_4(2050)$ as free parameters.

Here the unfolded differential cross sections are fitted. Fits are performed 1000 times for each study with randomly generated initial values for the parameters A unique

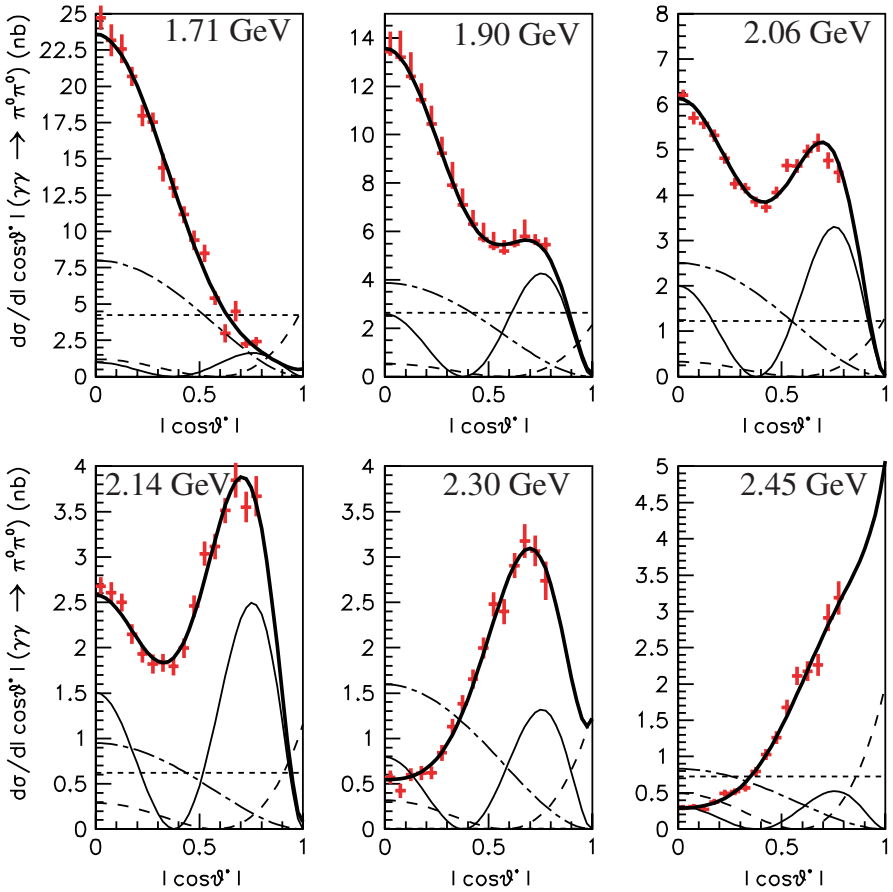

FIG. 6 (color online). Measurements of $d\sigma/d|\cos\theta^*|$ (nb) (data points) and results of the fit (thick solid lines) for the W bins indicated. The dotted, dashed, dot-dashed, and thin lines indicate $|S|^2$, $4\pi|D_0Y_2^0|^2$, $4\pi|D_2Y_2^2|^2$, and $4\pi|G_2Y_4^2|^2$, respectively.

solution with good quality ($\chi^2/ndf = 1.04$) is repeatedly found (''nominal fit''). The fit results are shown in Fig. 6 for the differential cross sections, in Fig. 7 for the total cross section, and in Figs. 4 and 5 for the $\hat{S}^2$, etc. Since the two-photon coupling of the $f_4(2050)$ has not been measured before, a fit without this resonance is also given in Table V. The fit quality is unacceptable, strongly indicating that the $f_4(2050)$ has a nonzero two-photon coupling. A fit without the ''$f_2(1950)$'' is also made giving a much worse fit and is included in Table V.

We have performed additional fits to investigate whether we can conclude that the $f_4(2050)$ is mainly produced in the helicity-2 state. Note that the angular dependence of Y_4^0 and Y_4^2 is very similar for $|\cos\theta^*| < 0.7$ and hence it is expected to be rather difficult to distinguish G_0 and G_2 waves. A fit where the role of G_0 and G_2 is interchanged [i.e., by setting $G_2 = 0$ and by including the $f_4(2050)$ and background in G_0] yields $\chi^2 = 448.2$, which can be compared to 323.2 for the nominal fit. However, more reasonable fits are obtained when two more parameters are introduced in the G_2 background (a second-order polynomial real amplitudes or linear amplitudes for both real and imaginary parts, which are set to zero at $W = 1.7$ GeV). Here the fits where the role of G_2 and G_0 have been interchanged are also compared. In each case, the $f_4(2050)$ in a G_2 wave is favored over that in a G_0 wave with χ^2 differences of about 6 and 26, respectively. Thus, the helicity-2 production of the $f_4(2050)$ is favored but not conclusively.

According to Fig. 7, the $|D_2|^2$ term has an enhancement around $W = 2.35$ GeV, which might be identified as the $f_2(2300)$. To study this possibility, a fit is made including the $f_2(2300)$. The conclusion is, however, that we have no sensitivity to it; the fit does not improve significantly by its inclusion. We believe that the enhancement arises from the ''$f_2(1950)$'' and its interference with the G_2 wave and underlying continuum, i.e., a fit without the ''$f_2(1950)$'' gives a smooth D_2 amplitude [with much worse χ^2 (Table V)].

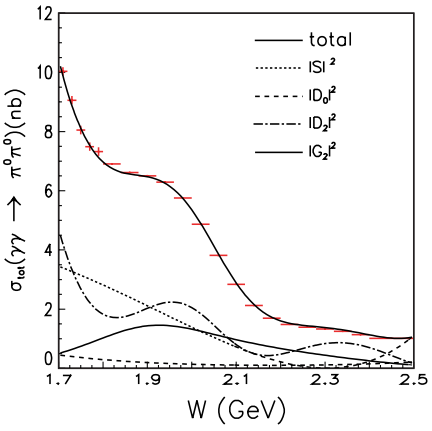

FIG. 7 (color online). Total cross section ($|\cos\theta^*| < 0.8$) (nb) and the results of the nominal fit (curves).

C. Study of systematic errors

Various sources of systematic errors on the parameters are considered such as dependence on the fitted region, normalization errors of the differential cross sections, assumptions on the background amplitudes, and uncertainties from the unfolding procedure.

For each study, a fit is made allowing all the parameters to vary. The differences of the fitted parameters from the nominal values are quoted as systematic errors. Again, 1000 sets of randomly generated input parameters are prepared for each study and fitted to search for the true minimum and for possible multiple solutions. Unique solutions are found repeatedly in all the cases. Once the solutions are found, several tens of repeated minimizations are needed to obtain fits that converge. With many parameters (24–26 here) to be fitted, the approach to the minimum is rather slow.

Two fitting regions are tried: a higher one (1.74 GeV $\leq W \leq$ 2.60 GeV) and a lower one (1.66 GeV $\leq W \leq$ 2.40 GeV). The normalization error studies are divided into those from uncertainties of the overall normalization and those from distortion of the spectra in both $|\cos\theta^*|$ and W. For the overall normalization errors, fits are made with differential cross sections multiplied by $(1 \pm \sigma_{\epsilon(W,|\cos\theta^*|)})$, where σ_ϵ is the relative efficiency error. For distortion studies, $\pm 4\%$ ($\pm 3\%$) errors are assigned over the $|\cos\theta^*|$ (W) range and differential cross sections are distorted by multiplying by $1 \pm 0.1|\cos\theta^*| \mp 0.04$ ($1 \pm 0.075W \mp 0.1575$).

For studies of the background (BG) amplitudes, each of the waves is changed to a first- or a third-order polynomial except for the G_0 wave, where a first-order polynomial is introduced for both the real and imaginary parts of the amplitude. Parametrization uncertainties due to the phase convention where the D_0 and G_2 background amplitudes are taken to be real are estimated by making the S and D_2 real instead and by introducing imaginary parts for the D_0 and D_2 terms.

The resulting systematic errors are summarized in Table VI. Total systematic errors are calculated by adding the individual errors in quadrature. We obtain the mass, total width, and $\Gamma_{\gamma\gamma}\mathcal{B}(\pi^0\pi^0)$ of the $f_4(2050)$ to be $1884^{+14+218}_{-13-25}$ MeV/c^2, $453 \pm 20^{+31}_{-129}$ MeV, and $7.7^{+1.2+23.5}_{-1.1-5.2}$ eV, where the first errors are statistical and the second systematic. The errors are dominated by systematics, and mostly come from uncertainties due to the unfolding procedure and background parametrization, and possible biases in the $\cos\theta^*$ distribution.

From the measured branching fraction to $\pi\pi$ (Table IV), the two-photon width of the $f_4(2050)$ is obtained to be $136^{+24+415}_{-22-91}$ eV. Given the large systematic error, we cannot conclude that the two-photon width of the $f_4(2050)$ is

TABLE VI. Systematic errors.

Source	$f_4(2050)$ Mass (MeV/c^2)	$f_4(2050)$ $\Gamma_{\rm tot}$ (MeV)	$f_4(2050)$ $\Gamma_{\gamma\gamma}\mathcal{B}_{\pi^0\pi^0}$ (eV)	"$f_2(1950)$" Mass (MeV/c^2)	"$f_2(1950)$" $\Gamma_{\rm tot}$ (MeV)	"$f_2(1950)$" $\Gamma_{\gamma\gamma}\mathcal{B}_{\pi^0\pi^0}$ (eV)
W range	$^{+6}_{-0}$	$^{+0}_{-28}$	$^{+4.3}_{-0}$	$^{+0}_{-14}$	$^{+0}_{-87}$	$^{+0}_{-27}$
Normalization	$^{+0}_{-2}$	$^{+0}_{-1}$	$^{+1.0}_{-0.8}$	$^{+2}_{-0}$	$^{+5}_{-0}$	$^{+11}_{-3}$
Bias: $\lvert\cos\theta^*\rvert$	$^{+15}_{-16}$	$^{+0}_{-0.7}$	$^{+2.7}_{-2.4}$	$^{+2}_{-0}$	$^{+5}_{-3}$	$^{+12}_{-3}$
Bias: W	$^{0}_{-1}$	± 1	± 0.2	$^{+3}_{-2}$	$^{+2}_{-0}$	$^{+1}_{-0}$
Unfolding	$^{+35}_{-0}$	$^{+0}_{-68}$	$^{+0}_{-3.0}$	$^{+0}_{-44}$	$^{+0}_{-84}$	$^{+0}_{-36}$
BG: ReS	$^{+50}_{-0}$	$^{+0}_{-72}$	$^{+0}_{-3.1}$	$^{+0}_{-46}$	$^{+9}_{-88}$	$^{+0}_{-37}$
BG: ImS	$^{+0}_{-1}$	$^{+2}_{-7}$	$^{+0}_{-0.1}$	± 1	$^{+9}_{-0}$	$^{+9}_{-0}$
BG: D_0	$^{+1}_{-13}$	$^{+9}_{-15}$	$^{+2.7}_{-0}$	$^{+3}_{-1}$	$^{+3}_{-4}$	$^{+22}_{-0}$
BG: ReD_2	$^{+36}_{-0}$	$^{+29}_{-2}$	$^{+11.9}_{-0.6}$	$^{+0}_{-22}$	$^{+24}_{-94}$	$^{+16}_{-24}$
BG: ImD_2	$^{+0}_{-12}$	$^{+0}_{-12}$	$^{+3.1}_{-0}$	$^{+0}_{-4}$	$^{+0}_{-13}$	$^{+11}_{-0}$
BG: G_0	$^{+20}_{-0}$	$^{+0}_{-23}$	$^{+0}_{-1.0}$	$^{+2}_{-21}$	$^{+6}_{-49}$	$^{+1}_{-19}$
BG: G_2	$^{+205}_{-0}$	$^{+7}_{-69}$	$^{+19.1}_{-0}$	± 10	$^{+0}_{-54}$	$^{+377}_{-13}$
BG: Real D_0 & G_2	± 6	$^{+1}_{-11}$	± 0.4	$^{+2}_{-1}$	$^{+1}_{-6}$	$^{+7}_{-6}$
Total	$^{+218}_{-25}$	$^{+31}_{-129}$	$^{+23.5}_{-5.2}$	$^{+12}_{-73}$	$^{+28}_{-192}$	$^{+379}_{-68}$

nonzero. However our data clearly require a G-wave component (see Fig. 6), and the unacceptable fit without the $f_4(2050)$ (Table V) strongly supports a finite two-photon coupling. In the past, TASSO and JADE have set 95% confidence upper limits for the $f_4(2050)$ to be $\Gamma_{\gamma\gamma}\mathcal{B}(KK) < 0.29$ keV [18] and $\Gamma_{\gamma\gamma}\mathcal{B}(\pi\pi) < 1.1$ keV [19], respectively. These can be translated into upper limits for the two-photon widths of 43 and 6.5 keV, respectively. The power of such a large statistics (3 orders of magnitude more) of our experiment is evident. The nominal fit brings quite unexpected results: it requires a "flip" of the $f_4(2050)$ and "$f_2(1950)$" positions with the mass of the former becoming 1885^{+14}_{-13} MeV or 153 MeV lower than the optimal mass of the "$f_2(1950)$". In addition, the fit requires both states to be much broader than before, 440–450 MeV or about 2 times larger than their PDG values. Obviously, the interference of the D_2 and G_2 amplitudes with each other and with the underlying continuum demands a more sophisticated description probably involving more than one resonance in each wave. Such a full amplitude analysis is beyond the scope of this work. On the other hand, results of all the fits provide unambiguous evidence for a nonzero two-photon coupling of the G wave.

V. ANALYSIS OF THE HIGHER-ENERGY REGION

In general, we expect that at high energies and large scattering angles, leading term QCD calculations give reasonable predictions for hard exclusive processes such as $\gamma\gamma \to M_1M_2$, where $M_{1(2)}$ are mesons. However, at what energies these terms begin dominating depends on the hadrons involved. In addition, even at the highest energies the differential cross sections depend on the shape of the $M_{1(2)}$ wave functions. For charged meson pairs such as $\pi^+\pi^-$, K^+K^-, the differential cross sections are only slightly sensitive to the shape of the wave functions and the numerically largest term in the differential cross sections is proportional to $\sin^{-4}\theta^*$ [9–11]. However for neutral meson pairs this term is absent; the cross section $d\sigma/d|\cos\theta^*|$ is much smaller and much more sensitive to the shape of the meson wave functions [9–11].

In contrast, the main idea of the handbag model [12] is that the terms that are asymptotically power corrections give the numerically largest contributions even at currently available energies. The universal prediction of the handbag model is that the ratios $d\sigma(M^0\bar{M}^0)/d\sigma(M^+M^-)$ are constant, i.e., the energy and angular dependences are the same for charged and neutral mesons. In particular, $d\sigma(\pi^0\pi^0)/d\sigma(\pi^+\pi^-) = 0.5$ [12] while it varies from ≈ 0.07 at $\cos\theta^* = 0$ to ≈ 0.04 at $|\cos\theta^*| = 0.6$ in Ref. [10].

A. Angular dependence

We compare the angular dependence of the differential cross sections in the range $|\cos\theta^*| < 0.8$ for $W > 2.4$ GeV with the function $\sin^{-4}\theta^*$. We also try a fit with an additional $\cos^2\theta^*$ term, to quantify a possible deviation from the $\sin^{-4}\theta^*$ behavior. We choose this function because it gives relatively good fits over a wide range in W. Thus the fit function is parametrized as

$$d\sigma/d|\cos\theta^*| = a(\sin^{-4}\theta^* + b\cos^2\theta^*). \quad (9)$$

We fit using a binned maximum likelihood method and 16 bins in the range $|\cos\theta^*| < 0.8$. We know that the effect of charmonia is large in the region 3.3 GeV $< W <$ 3.6 GeV, but we cannot separate it in the angular dependence be-

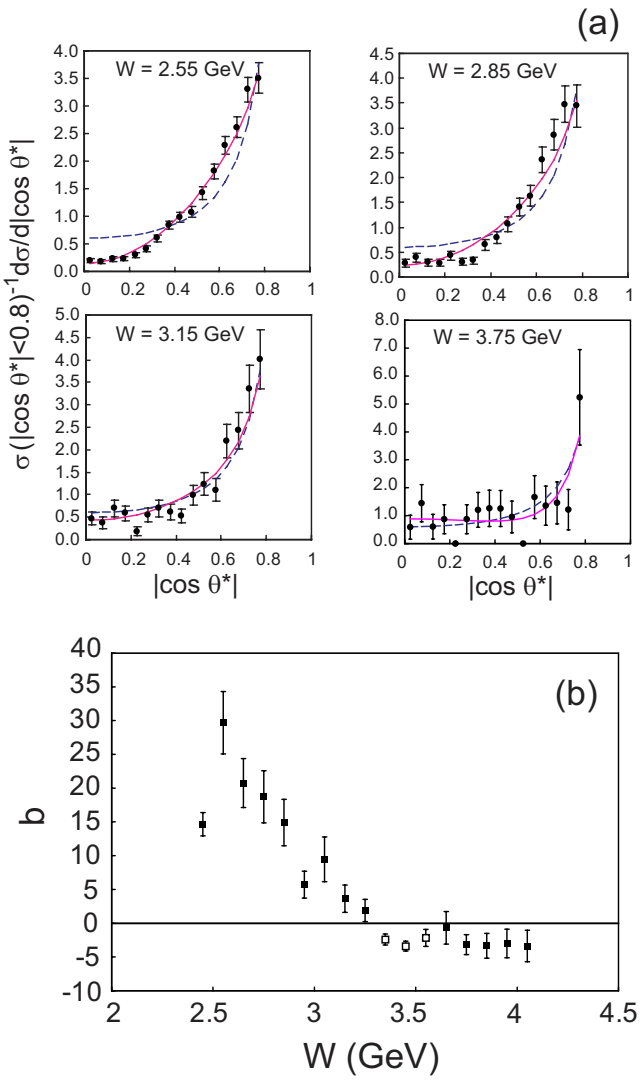

FIG. 8 (color online). (a) The fits of the angular dependence of the normalized differential cross sections (see text) at four selected W points. For the dashed curves the coefficient b (see the fit formula in the text) is fixed to 0. The solid curves show the fits with b floating. (b) The energy dependence of the parameter b giving the best fits. Here, the charmonium contributions are not subtracted, and the data in the χ_{c0} and χ_{c2} charmonium regions are plotted with open squares.

cause we cannot assume here any functional shapes for the noncharmonium component. The results of the fit for b are shown in Fig. 8, as well as the fit to the angular distributions in the four selected W regions, where the differential cross sections, the vertical axis of this figure, are normalized to the total cross section $\sigma(|\cos\theta^*| < 0.8)$ in each W region, i.e., the area under the curve is 1. The parameter b is close to zero above $W > 3.1$ GeV compared to $b \sim 10$, when the contribution of the $b\cos^2\theta^*$ term in the total cross section, $\sigma(|\cos\theta^*| < 0.8)$, is comparable to the contribution of the $\sin^{-4}\theta^*$ term. The b parameter becomes nearly constant and then systematically negative above the charmonium region. The change in the b parameter, which approaches a constant value near zero, occurs at a W value close to that observed in the charged-pion case [2].

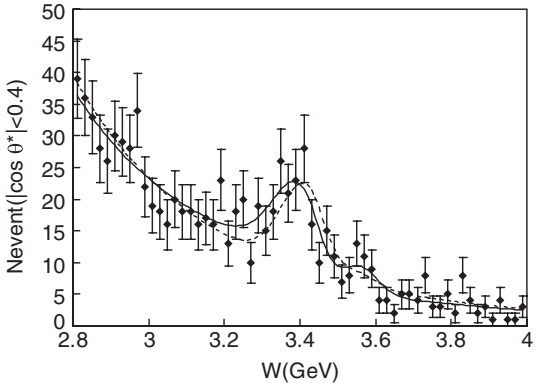

FIG. 9. The W distribution of the candidate events with $|\cos\theta^*| < 0.4$ near the charmonium region. The solid and dashed curves show the fits described in the text with and without interference with the χ_{c0}.

B. Yields of χ_{cJ} charmonia

The structures seen in the yield distribution for 3.3 GeV $< W <$ 3.6 GeV and $|\cos\theta^*| < 0.4$ (Fig. 9) are from charmonium production, $\gamma\gamma \to \chi_{c0}$, $\chi_{c2} \to \pi^0\pi^0$. Similar production of the two charmonium states is observed in the $\pi^+\pi^-$, K^+K^-, and $K^0_S K^0_S$ final states [2,4].

We fit the distribution to contributions from the χ_{c0}, χ_{c2} and a smooth continuum component using the following function:

$$Y(W) = |\sqrt{\alpha k W^{-\beta}} + e^{i\phi}\sqrt{N_{\chi_{c0}}}\mathrm{BW}_{\chi_{c0}}(W)|^2 + N_{\chi_{c2}}|\mathrm{BW}_{\chi_{c2}}(W)|^2 + \alpha(1-k)W^{-\beta}, \quad (10)$$

in the W region between 2.8 and 4.0 GeV, where $\mathrm{BW}_{\chi_{cJ}}(W)$ is a Breit-Wigner function for the charmonium amplitude, which is proportional to $1/(W^2 - M^2_{\chi_{cJ}} - iM_{\chi_{cJ}}\Gamma_{\chi_{cJ}})$ and is normalized as $\int|\mathrm{BW}_{\chi_{cJ}}(W)|^2 dW = 1$. The masses and widths, M and Γ, of the charmonium states are fixed to the PDG world averages [17]. The component $\alpha W^{-\beta}$ corresponds to the contribution from the continuum, with a fraction k that interferes with the χ_{c0} amplitude with a relative phase angle, ϕ. It is impossible to determine the interference parameters for the χ_{c2} because of its much smaller intrinsic width compared to experimental resolution. We fit the χ_{c2} yield ($N_{\chi c2}$) with a formula where no interference term is included, and later we estimate the maximum effects from the interference term when determining the two-photon decay width of χ_{c2}. We use data only in the range $|\cos\theta^*| < 0.4$ where the charmonium contribution is dominant. Smearing effects due to a finite mass resolution are taken into account in the fit, using the same function as used for the unfolding.

TABLE VII. Results of the fits (see text) to obtain the charmonium contributions with and without interference effects. Errors are statistical only. Logarithmic likelihood ($\ln\mathcal{L}$) values are only meaningful when comparing two or more fits.

Interference	$N_{\chi_{c0}}$	k	ϕ	$N_{\chi c2}$	$-2\ln\mathcal{L}/ndf$
Without	100 ± 16	...	...	13^{+11}_{-10}	52.4/56
With	103^{+60}_{-42}	$0.82^{+0.18}_{-0.48}$	$(1.1 \pm 0.3)\pi$	34 ± 13	44.2/54

A binned maximum likelihood method is applied. We examined two cases with and without the interference. Reasonably good fits are obtained for both cases. The fit results are summarized in Table VII. In the table, $\mathcal{L}$ is the likelihood value and ndf is the number of degrees of freedom. The normalization $N_{\chi c0}$ in Eq. (8) is proportional to the square of the resonance amplitude. The yields from the fits are translated into products of the two-photon decay width and the branching fraction, $\Gamma_{\gamma\gamma}(\chi_{cJ})\mathcal{B}(\chi_{cJ} \to \pi^0\pi^0)$, which are listed in Table VIII. The systematic errors are taken from the changes in the central values of the fitted yields when the absolute energy scale is varied by ± 10 MeV for the W measurement, the invariant-mass resolution is varied by $\pm 10\%$ for the corresponding Gaussian widths, and the fitting range is narrowed to the range 2.96–3.84 GeV, and when the efficiencies are varied by their uncertainties. The changes in the goodness of fit ($-2\ln\mathcal{L}$) for the first two variations are found to be small, less than 1.7, for the interference case.

The χ_{c0} is observed with a statistical significance of 7.6σ (7.3σ) when we take (do not take) interference into account. The statistical significance for the χ_{c2} is 2.6σ when we take interference of the χ_{c0} into account, but it is only 1.3σ when we do not take into account interference. This is because interference makes the line shape of the χ_{c0} highly asymmetric with a short tail and destructive interference on the high-energy side. The solid and dashed curves in Fig. 9 show the fits for the two cases (with and without χ_{c0} interference).

The results for $\Gamma_{\gamma\gamma}\mathcal{B}(\chi_{cJ})$ in the $\pi^0\pi^0$ final state can be compared to the only direct measurement of this quantity in the $\pi^+\pi^-$ decay mode from Belle, $15.1 \pm 2.1 \pm 2.3$ eV and $0.76 \pm 0.14 \pm 0.11$ eV for the χ_{c0} and χ_{c2}, respectively [2]. Although the effects of interference were neglected in the $\pi^+\pi^-$ measurements, the results are consistent with the ratio expected from isospin invariance, $\mathcal{B}(\chi_{cJ} \to \pi^0\pi^0)/\mathcal{B}(\chi_{cJ} \to \pi^+\pi^-) = 1{:}2$. Our results for $\Gamma_{\gamma\gamma}\mathcal{B}(\chi_{cJ})$ for the $\chi_{c0(2)}$ agree within errors with the indirect determination of these quantities using the corresponding world averages [17] or recent measurements of $\mathcal{B}(\chi_{c0(2)} \to \pi^0\pi^0)$ [20] as well as $\mathcal{B}(\chi_{cJ} \to \gamma\gamma)$ and $\Gamma_{\gamma\gamma}(\chi_{cJ})$ [21] by the CLEO Collaboration.

TABLE VIII. Products of the two-photon decay width and the branching fraction for the two charmonia. Here, $\Gamma_{\gamma\gamma}\mathcal{B}(\chi_{cJ})$ means $\Gamma_{\gamma\gamma}(\chi_{cJ})\mathcal{B}(\chi_{cJ} \to \pi^0\pi^0)$. The first, second, and third errors (when given) are statistical, systematic, and from the maximal uncertainties of the relative phase in χ_{c2} production.

Interference	$\Gamma_{\gamma\gamma}\mathcal{B}(\chi_{c0})$ (eV)	$\Gamma_{\gamma\gamma}\mathcal{B}(\chi_{c2})$ (eV)
Without	$9.7 \pm 1.5 \pm 1.2$	$0.18^{+0.15}_{-0.14} \pm 0.08$
With	$9.9^{+5.8}_{-4.0} \pm 1.6$	$0.48 \pm 0.18 \pm 0.07 \pm 0.14$

C. Subtraction of the charmonium contributions

We subtract the charmonium contributions from nearby bins of the charmonium (χ_{cJ}) region, 3.3–3.6 GeV, in order to obtain a pure differential cross section from the continuum component. We use the fit result with interference obtained in the previous section.

The estimated charmonium yield that includes the contribution from the interference term is converted to a differential cross section contribution in each angular bin of $|\cos\theta^*| < 0.8$ by assuming a flat distribution for the χ_{c0} component and a distribution $\sim\sin^4\theta^*$ for the χ_{c2} component [4]. This assumption is only a model. In fact, we do not know the angular distribution of the interference term; the charmonium amplitudes can interfere with the continuum components with different J's of unknown sizes.

For the $W = 3.25$ GeV bin, the fit result indicates that there is a non-negligible effect from the χ_{c0} when we assume interference, and thus we make a correction for charmonium subtraction. The contribution of the charmonium components in the original differential cross sections is 18% at $|\cos\theta^*| < 0.6$. For $W = 3.3$–3.6 GeV, we apply a subtraction for the angular bins $0.4 < |\cos\theta^*| < 0.8$ after extrapolating the charmonium yield determined in the range $|\cos\theta^*| < 0.4$.

The differential cross section thus obtained for the continuum is integrated over the range $|\cos\theta^*| < 0.6$. We convert $\sigma(0.4 < |\cos\theta^*| < 0.8)$ to $\sigma(|\cos\theta^*| < 0.4)$ for $W = 3.2$–3.6 GeV, by assuming that the angular dependence of the differential cross section is $\sim\sin^{-4}\theta^*$. The results are plotted in Fig. 10(a), where the cross section for $\gamma\gamma \to \pi^+\pi^-$ from Ref. [2] is also shown.

D. W dependence and ratio of cross sections of $\pi^0\pi^0$ to $\pi^+\pi^-$

We fit the differential cross sections integrated over the polar angle, $\sigma(|\cos\theta^*| < 0.6)$, to a power law in the c.m. energy, W^{-n}, for the energy region $3.1\ \text{GeV} < W < 4.1$ GeV, in which the angular dependence of the differential cross section does not show any large changes. In the

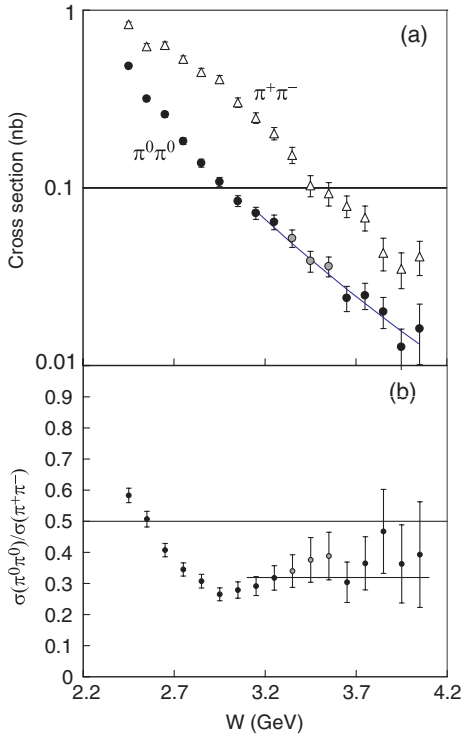

FIG. 10 (color online). (a) The cross sections for the $\gamma\gamma \to \pi^0\pi^0$ (solid circles) and $\gamma\gamma \to \pi^+\pi^-$ (triangles, [2]) for $|\cos\theta^*| < 0.6$. The curve is a fit to the cross section for $\gamma\gamma \to \pi^0\pi^0$ with a $\sim W^{-n}$ functional shape. (b) Ratio of the cross section for the $\pi^0\pi^0$ process to the $\pi^+\pi^-$ process. The error bars are statistical only. The shorter horizontal line is the average for 3.1 GeV $< W <$ 4.1 GeV. The horizontal line (0.5) is an expectation from isospin invariance for a pure $I = 0$ component. In (a) and (b), the estimated charmonium contributions are subtracted in both $\pi^+\pi^-$ and $\pi^0\pi^0$ measurements. The results in the W region 3.3–3.6 GeV (plotted with gray circles) are not used for the fits.

fit, we do not use the data in the charmonium region ($W =$ 3.3–3.6 GeV), where we cannot determine the cross section of the continuum component in a model-independent manner.

The result of the power-law fit is summarized in Table IX and compared to that for other processes. The systematic error is dominated by the uncertainty of the charmonium contribution in the range 3.1 GeV $< W <$ 3.3 GeV. This n value is compatible with the results for the $\pi^+\pi^-$ and K^+K^- processes [2], but significantly smaller than that in the $K^0_S K^0_S$ case [4].

The fit for 3.1 GeV $< W <$ 4.1 GeV is shown in Fig. 10(a), which also shows the cross section of $\pi^0\pi^0$ from the Belle measurement [2]. In Fig. 10(b) we show the ratio of the cross sections of $\pi^0\pi^0$ to $\pi^+\pi^-$. This ratio is rapidly falling at low energies, but its behavior changes above 3.1 GeV, where the two processes have similar W^{-n} dependence, which results in the almost constant ratio. The average of the ratio in this energy region is $0.32 \pm 0.03 \pm 0.05$, where the data in the 3.3–3.6 GeV region are not used when calculating this average. This ratio is significantly larger than the prediction of the leading-order QCD calculations [9–11] and is somewhat smaller than the value of 0.5, which is suggested by isospin invariance [12].

VI. SUMMARY AND CONCLUSION

We have measured the process $\gamma\gamma \to \pi^0\pi^0$ using a high-statistics data sample from e^+e^- collisions corresponding to an integrated luminosity of 223 fb^{-1} collected with the Belle detector at the KEKB accelerator. We derive results for the differential cross sections in the center-of-mass energy and polar angle ranges, 0.6 GeV $< W <$ 4.1 GeV and $|\cos\theta^*| < 0.8$.

Differential cross sections are fitted in the energy region 1.7 GeV $< W <$ 2.5 GeV in a model where the partial waves consist of resonances and smooth backgrounds. Various fits are performed that provide unambiguous evidence for a nonzero two-photon coupling of the G wave. Helicity-2 production (G_2) is preferred compared to the helicity-0 (G_0) one.

We observe production of the charmonium state χ_{c0} and obtain the product of its two-photon decay width and the branching fraction to $\pi^0\pi^0$. The angular distribution of the differential cross section is largely energy dependent, and approaches $\sim\sin^{-4}\theta^*$ above $W = 3.1$ GeV. This observation and the energy dependence of the cross section above this energy, which is well fitted by W^{-n}, $n = 6.9 \pm 0.6 \pm 0.7$, are compatible with those measured in the $\pi^+\pi^-$ channel. We obtain the cross section ratio, $\sigma(\pi^0\pi^0)/\sigma(\pi^+\pi^-)$, to be $0.32 \pm 0.03 \pm 0.05$ on average in the 3.1–4.1 GeV region. This ratio is significantly larger than the prediction of the leading-order QCD calculation.

TABLE IX. The value n in $\sigma_{\rm tot} \propto W^{-n}$ in various reactions fitted in the W and $|\cos\theta^*|$ ranges indicated.

Process	n	W range (GeV)	$\lvert\cos\theta^*\rvert$ range	Reference
$\pi^0\pi^0$	$6.9 \pm 0.6 \pm 0.7$	3.1–4.1 (exclude 3.3–3.6)	<0.6	This expt.
$\pi^+\pi^-$	$7.9 \pm 0.4 \pm 1.5$	3.0–4.1	<0.6	[2]
K^+K^-	$7.3 \pm 0.3 \pm 1.5$	3.0–4.1	<0.6	[2]
$K^0_S K^0_S$	$10.5 \pm 0.6 \pm 0.5$	2.4–4.0 (exclude 3.3–3.6)	<0.6	[4]
$\pi^0\pi^0$	$8.0 \pm 0.5 \pm 0.4$	3.1–4.1 (exclude 3.3–3.6)	<0.8	This expt.

ACKNOWLEDGMENTS

We are grateful to V. Chernyak for useful discussions. We thank the KEKB group for the excellent operation of the accelerator, the KEK cryogenics group for the efficient operation of the solenoid, and the KEK computer group and the National Institute of Informatics for valuable computing and SINET3 network support. We acknowledge support from the Ministry of Education, Culture, Sports, Science, and Technology (MEXT) of Japan, the Japan Society for the Promotion of Science (JSPS), and the Tau-Lepton Physics Research Center of Nagoya University; the Australian Research Council and the Australian Department of Industry, Innovation, Science and Research; the National Natural Science Foundation of China under Contracts No. 10575109, No. 10775142, No. 10875115, and No. 10825524; the Department of Science and Technology of India; the BK21 program of the Ministry of Education of Korea, the CHEP src program and Basic Research program (Grant No. R01-2008-000-10477-0) of the Korea Science and Engineering Foundation; the Polish Ministry of Science and Higher Education; the Ministry of Education and Science of the Russian Federation and the Russian Federal Agency for Atomic Energy; the Slovenian Research Agency; the Swiss National Science Foundation; the National Science Council and the Ministry of Education of Taiwan; and the U.S. Department of Energy. This work is supported by a Grant-in-Aid from MEXT for Science Research in a Priority Area (''New Development of Flavor Physics''), and from JSPS for Creative Scientific Research (''Evolution of Tau-lepton Physics'').

[1] T. Mori *et al.* (Belle Collaboration), J. Phys. Soc. Jpn. **76**, 074102 (2007); Phys. Rev. D **75**, 051101(R) (2007).
[2] H. Nakazawa *et al.* (Belle Collaboration), Phys. Lett. B **615**, 39 (2005).
[3] K. Abe *et al.* (Belle Collaboration), Eur. Phys. J. C **32**, 323 (2004).
[4] W. T. Chen *et al.* (Belle Collaboration), Phys. Lett. B **651**, 15 (2007).
[5] C. C. Kuo *et al.* (Belle Collaboration), Phys. Lett. B **621**, 41 (2005).
[6] S. Uehara *et al.* (Belle Collaboration), Phys. Rev. Lett. **96**, 082003 (2006).
[7] S. Uehara *et al.* (Belle Collaboration), Phys. Rev. D **78**, 052004 (2008).
[8] See, e.g., the compilation in http://durpdg.dur.ac.uk/spires/hepdata/online/2gamma/2gammahome.html.
[9] S. J. Brodsky and G. P. Lepage, Phys. Rev. D **24**, 1808 (1981).
[10] M. Benayoun and V. L. Chernyak, Nucl. Phys. **B329**, 285 (1990).
[11] V. L. Chernyak, Phys. Lett. B **640**, 246 (2006).
[12] M. Diehl, P. Kroll, and C. Vogt, Phys. Lett. B **532**, 99 (2002).
[13] A. Abashian *et al.* (Belle Collaboration), Nucl. Instrum. Methods Phys. Res., Sect. A **479**, 117 (2002).
[14] S. Kurokawa and E. Kikutani, Nucl. Instrum. Methods Phys. Res., Sect. A **499**, 1 (2003), and other papers included in this volume.
[15] S. Uehara, KEK Report No. 96-11 1996.
[16] A. Höcker and V. Kartvelishvili, Nucl. Instrum. Methods Phys. Res., Sect. A **372**, 469 (1996).
[17] C. Amsler *et al.* (Particle Data Group), Phys. Lett. B **667**, 1 (2008).
[18] M. Althoff *et al.* (TASSO Collaboration), Z. Phys. C **29**, 189 (1985).
[19] T. Oest *et al.* (JADE Collaboration), Z. Phys. C **47**, 343 (1990).
[20] D. M. Asner *et al.* (CLEO Collaboration), arXiv:0811.0586.
[21] K. M. Ecklund *et al.* (CLEO Collaboration), Phys. Rev. D **78**, 091501 (2008).